Journal of the European Ceramic Society 22 (2002) 1553–1567

www.elsevier.com/locate/jeurceramsoc

Processing of Al_2O_3/SiC nanocomposites—part 1: aqueous colloidal processing

L.A. Timms*,[1], C.B. Ponton

IRC in Materials and School of Metallurgy and Materials, The University of Birmingham, Edgbaston, Birmingham B15 2TT, UK

Received 26 April 2001; received in revised form 22 August 2001; accepted 19 September 2001

Abstract

An aqueous sol preparation route was investigated for the production of Al_2O_3/SiC nanocomposites. Different alumina and silicon carbide powders were used as well as two polyelectrolyte dispersing agents. The alumina powders were dispersed first, via wet ball milling, with silicon carbide being added during a second milling stage. Dispersed sols were prepared with silicon carbide powders having an average particle size ranging from 0.5 μm down to 50 nm. The rheological characteristics of the sols were determined and used together with the results from TEM studies of the sols to ascertain the spatial arrangement of sol particles or 'sol architecture'. It was found that whilst a polydispersion approach is suitable for the coarser SiC powders, this cannot be applied to very fine particles. Rather, the pH of the sol has to be lowered to encourage heterocoagulation.

Keywords: Al_2O_3–SiC; Dispersion; Milling; Nanocomposites; Suspensions

1. Introduction

The potential for ceramic nanocomposites to offer significantly enhanced mechanical properties was discovered through the work of Niihara.[1] Many studies have now been performed, investigating problems such as the dispersion of the fine second phase and the mechanisms behind property enhancement. The work presented here is concerned with the processing of alumina/silicon carbide nanocomposites via aqueous colloidal processing and forms Part 1 of a two-part investigation. Part 2 provides details on green body formation and the microstructure obtained using a pressureless sintering route.

Original work by Niihara's group reports on the use of various organic liquids as the dispersing medium, such as ethanol,[1] toluene[2] and acetone.[3] Stearns et al.[4] carried out an in depth study on processing with non-aqueous media in response to the relatively little detail provided on processing procedures by Niihara and co-workers. They found methanol to be a suitable dispersing medium, which has been used by other workers such as Conder[5] and O'Sullivan et al.[6] Amongst the various liquids studied by Stearns et al.,[4] hexane was found to be the least effective dispersing medium. Conder[5] reported that toluene was also a very poor dispersing medium; both toluene and hexane are non-polar molecules.

The main drawback associated with *aqueous* processing is the occurrence of hard agglomerates on drying of the slurry.[4] In response to these concerns, Walker et al.[7] investigated different drying methods, and found that freeze drying avoided the formation of hard agglomerates. It was also found that pH adjustment could be used to induce flocculation of the slurry, preventing segregation and agglomeration of the silicon carbide particles. However, in the present work pressure filtration was used to form the green body (details can be found in Part 2 of this two-part investigation). This shaping technique allows the composite sol to remain in its dispersed state prior to forming and thus avoids the necessity for slurry drying. Consequently, the emphasis here lies in the control of the surface chemistry of the powder particles in the slurry. This will affect the arrangement of particles or 'sol architecture'.

Aslan et al.[8] investigated the possibilities of producing both heterocoagulated and polydispersed slurries. Heterocoagulated systems were prepared by dispersing the alumina and silicon carbide separately in water, and then combining them at pH = 4. O'Sullivan et al.[6] adopted a similar approach using water at pH = 6. At such low pH levels the zeta potentials of the two powders are opposite in sign and so there is electrostatic attraction

* Corresponding author.
E-mail address: lee.timms@ntlworld.com (L.A. Timms).
[1] Now at: EDS, Bartley Wood Business Park, 7 Bartley Way, Hook, Hampshire RG27 9NA, UK.

0955-2219/02/$ - see front matter
PII: S0955-2219(01)00465-4

between the silicon carbide and the alumina surfaces. Aslan et al.[8] re-dispersed these heterocoagulated particles by adding 2 wt.% of a non-ionic polymer, with the application of ultrasonic agitation. It is thought that the polymer acted as a steric barrier around the heterocoagulated particles to limit the magnitude of the electrostatic attraction between the clusters. Polydispersed systems were prepared first by modifying the surface chemistry of the silicon carbide using aminoethyl aminopropyl trimethoxysilane. This shifts the isoelectric point (IEP) to a higher pH value, imparting an overall positive charge to the silicon carbide surface, allowing well-dispersed slurries to be prepared over a pH range of 2 to 5. The two powders were then mixed in an attrition mill in the presence of a polymeric acid.

A more extensive study of the polydispersed system developed by Aslan et al.[8] was carried out later by Assmann et al.,[9] who examined the effect of varying the proportions of alumina and silicon carbide. As the volume percent of silicon carbide was increased, the attainable solids volume loading of the slurry decreased due to an increase in viscosity, with a maximum solids volume loading of 44 vol.% being obtained for a 5 vol.% Al_2O_3/SiC nanocomposite. This behaviour is attributed to a specific interaction of the modified silicon carbide surface with the polymeric acid; namely poly acrylic acid (PAA), with an average molecular weight of 1000. Agglomerates of silicon carbide were also found and so a second system was developed to ensure a more homogeneous distribution. The second system employed a small non-ionic organic molecule in the place of the PAA at pH = 5 (a necessary condition for the molecule to function effectively). The solids loading of the slurries could then be increased to 47 vol.%, regardless of silicon carbide content and showed reduced shear thinning behaviour compared with the PAA system. Green densities of 62% TD were achieved for 5 vol.% SiC composites via slip casting.

Modifications to the surface charge of silicon carbide have also been performed by Baklouti et al.,[10] to generate a polydispersed system. The surface of the powder was modified by adding poly ethylene imine (PEI), under conditions of low pH (average molecular weight of PEI: 50,000). Addition of a strong acid neutralises the NH basic groups, giving rise to a positive charge on the polymer. Good dispersions of silicon carbide were obtained for 3 wt.% PEI, with 70% neutralisation of the polymer, at pH = 3. The NH_2^+ groups are able to link with the negative sites on the particle surface, giving an overall positive charge. Nanocomposite slurries were then obtained by mixing a slurry of silicon carbide with an alumina slurry, also prepared at pH = 3.

The colloidal processing of the nanocomposites developed in the present work is based upon the use of a polyelectrolyte dispersant to stabilise the slurries during the milling stages. Polyelectrolytes are polymers with a net electrostatic surface charge and allow high volume loading sols to be prepared because they produce both an electrostatic barrier to agglomeration, as well as a steric barrier. This is important for achieving high density during pressure filtration. High green densities are vital to obtaining dense material via a pressureless sintering route when faced with second phase inclusions that retard densification during sintering.

2. Experimental procedure

2.1. Materials

α-Alumina powders were obtained from Baikalox, France (type CR15) and Alcan, England (type RA207LS). The Baikalox powder is produced by the crystallisation of alum ($Al_2(SO_4)_3{\cdot}(NH_4)_2SO_4{\cdot}24H_2O$), followed by thermal decomposition to obtain γ-alumina. The γ-alumina is then converted to α-alumina by a second thermal treatment. Jet milling is used to break down hard agglomerates produced during the calcination stage, giving rise to a fine powder. The Alcan powder is prepared by the refining of Bauxite via the Bayer process, followed by comminution to reduce the particle size. The Alcan powder was chosen to represent a typical sinter-active alumina and the Baikalox powder for its very high sinter-activity. It was anticipated that the latter might be necessary when dealing with the combined limitations of pressureless sintering and second phase inclusions.

The silicon carbide was supplied from two different sources; namely: H.C. Starck, Germany (types UF 15, UF 32 and UF 45) and ENEA, Italy. The figures in the names on the H.C. Starck materials refer to the surface area of the powders (in m^2/g). The H.C. Starck powders were α-silicon carbide, produced via the Acheson process, which is based on the carbothermal reduction of silica. Mechanical grinding is then used to reduce the particle size of the powders. An ultra-fine, β-silicon carbide was obtained from ENEA, Italy on a collaborative research basis. ENEA quote the specific surface area of the powder to be 80 m^2/g. The SiC is produced by a CO_2 laser induced gas phase reaction.[11] The laser is focused at the centre of a reaction cell (at approximately 1500 °C and 70 kPa), where it intersects the silane and ethene gas streams to produce silicon carbide and hydrogen gas. The silicon carbide used here was C-rich, having 32 wt.% C, 63 wt.% Si and 4 wt.% O.

2.2. Colloidal processing

The present work was limited to the preparation of 5 vol.% silicon carbide nanocomposites. In order to produce the required intra/inter-granular nanocomposite microstructure it is important to obtain a good dispersion of the silicon carbide particles throughout the

composite slurry. Soft agglomerates, which will inevitably be present in the commercial powders, must be broken down and the resulting sol stabilised. Wet ball milling was therefore used as an important first processing step.

Alumina slurries were prepared from de-ionized water and a dispersant, with yttria-tetragonal zirconia polycrystal (Y-TZP) milling media. The slurry was added to occupy 35 vol.% of the polyethylene bottle, the milling media occupying a level corresponding to half the height of the container (30 vol.% of the bottle).

The dispersant used was either Dispex A40 or Versicol K11 (Allied Colloids, UK), both of which are electrosteric-dispersing agents, whose chemical structures are shown in Fig. 1. Dispex A40 is an ammonium salt of poly acrylic acid or PAA-A, with an average molecular weight in the range 3000 to 3500. When added to a sol the organic part of the salt can adsorb onto particle surfaces and thus give a steric barrier to coagulation. Dissociation of the ammonium ions from the polymer chain also gives rise to an electrostatic barrier since the adsorbed polymer is left with negatively charged (COO^-) groups along its length. Versicol K11 is 3 parts poly methacrylic acid or PMAA and 1 part PAA, with a molecular weight of approximately 10,000. PMAA is similar to PAA-A in having carboxylic acid sites/functional groups along its length, but it has not been neutralised by ammonium hydroxide to give the salt form. Depending on the solvent conditions (i.e. pH and ionic strength), the fraction of functional groups that are dissociated (COO^-) and non-dissociated (COOH) varies. Consequently, the polymer surface charge will vary from relatively neutral to highly negative as the number of dissociated groups increases.

2.2.1. Wet ball milling trials on alumina powders

The milling process was examined in order to determine a suitable comminution period using a nominal amount of dispersant. Milling progress was monitored by measuring the pH, particle size distribution (PSD) and viscosity of the slurries. Particle size analysis was performed using a laser light diffraction technique (Coulter LS130). Viscosity measurements were performed using a controlled stress rheometer (Carri-Med CSL 500), with cone and plate geometry.

Fig. 2 shows a TEM micrograph of the milled CR15 powder, showing some very fine, 70 nm particles as well as larger, 0.25 μm particles. There is strong evidence of the calcination treatment used to produce the α-phase from the rounded appearance of the particles. The large angular particle in the top right of the micrograph has probably formed from a larger grain during the milling stage. There are also some hard agglomerates formed between several of the smaller particles which have

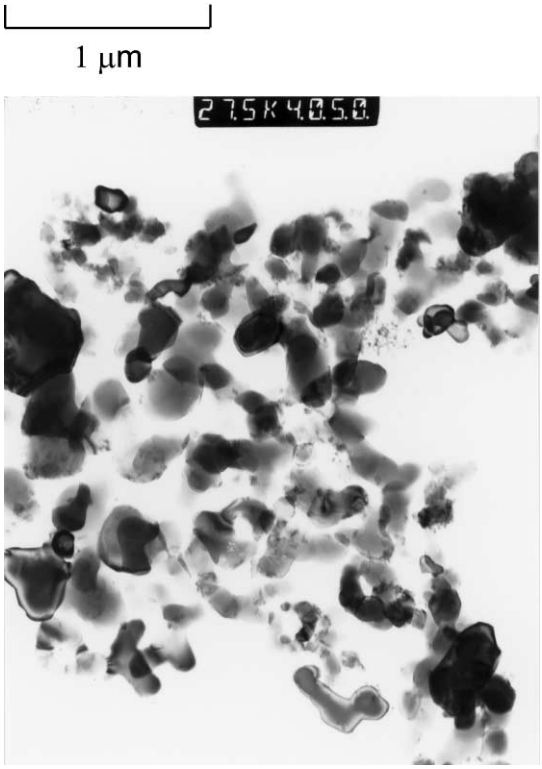

Fig. 2. TEM micrograph of the CR15 powder after milling for 40 h.

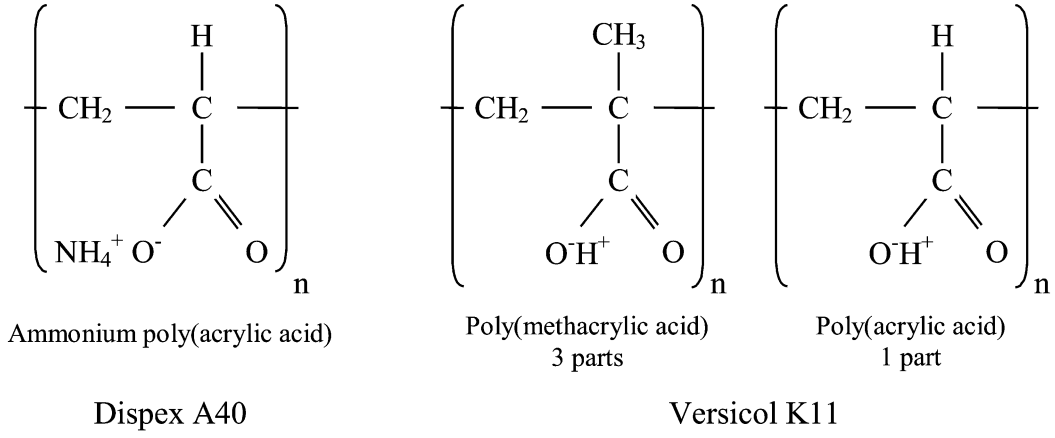

Fig. 1. The chemical structure of Dispex A40 and Versicol K11.

sintered together during the treatment; such as the 'L' shaped particle in the middle left of the micrograph. The largest dimension of this particle, in the plane of the micrograph, is 0.5 μm and is unlikely to be broken down during the milling. The TEM micrograph of the RA207LS powder in Fig. 3 reveals a more angular particle morphology, as a result of the comminution process used during powder production. Although specified as a sinter-active powder, the RA207LS is obviously coarser than the CR15 material.

2.2.2. Optimisation of alumina slurry rheology

The effect of the amount of dispersant (Versicol K11) on the viscosity of milled CR15 and RA207LS slurries at a fixed pH was investigated in order to determine the optimum content for the slurry batches. The pH was fixed at just above pH = 9 by adding ammonia, to promote the action of the dispersant most effectively;[12] the actual values were 9.1 ± 0.1 and 9.4 ± 0.1 for the RA207LS and CR15 systems, respectively. The amount of dispersant, expressed in wt.%, was measured on a dry weight of alumina powder basis. A range of 0.5 to 2.4 wt.% and 0.5 to 6.0 wt.% Versicol K11 were used for RA207LS and CR15, respectively. The difference in the range of the amount of dispersant used was based on the different surface areas of the two powders. Owing to the higher surface area of the CR15 powder, the maximum slurry solids loading that could be used, without creating a slurry with too high a viscosity, was less than that for the RA207LS. The RA207LS slurries were prepared at 50 ± 1 vol.% solids loading, compared with a solids loading of 37 ± 1 vol.% achieved for the CR15 powder.

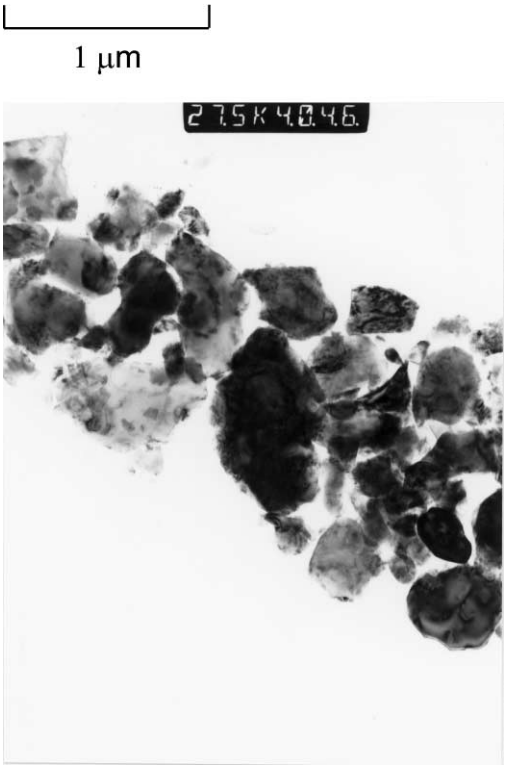

Fig. 3. TEM micrograph of the RA207LS powder after milling for 40 h.

2.2.3. Slurry batch production of nanocomposites

Once a suitable milling period and optimum amount of dispersant were identified for the alumina sols, slurry batch production was commenced for the production of green samples. This involved milling the alumina followed by the addition of silicon carbide in two stages, adding approximately equal amounts at each stage. The slurry was milled for 1 and 2 h, after the first and second additions, respectively. Milling was used to aid the mixing and dispersion process through the breakdown of soft agglomerates in the silicon carbide powder. The viscosity and the volume percent of solids were measured in order to compare the colloidal states of the slurries and as a method of 'quality control'. A breakdown of the slurry batches produced is given in Table 1.

For the case of the nanocomposites containing H.C. Starck silicon carbide, no further additions of water were required when adding the second phase. However, the processing of the nanocomposite slurries containing the silicon carbide manufactured by ENEA was more involved.

The preparation of the alumina slurry remained unchanged, but the addition of the silicon carbide required further amounts of water to keep the viscosity to an acceptable level for subsequent milling. This is due to the much larger surface area of the ENEA silicon carbide adsorbing a larger volume of water, compared with the types manufactured by H.C. Starck. The SL/Q1 slurry was processed, as normal, at a high pH of around 9, while the SL/Q2 slurry pH was adjusted prior to silicon carbide addition, to a low pH of 5.6 ± 0.2. This followed preliminary investigations where mass segregation of the silicon carbide and alumina could be witnessed in sols processed at a high pH. The problem was never apparent in the case of the silicon carbide

Table 1
Details of the slurry batches used to produce green samples

Slurry name	Alumina type	Silicon carbide type
SL/J	Alcan, RA207LS	H.C. Starck, UF15
SL/K	Baikalox, CR15	H.C. Starck, UF15
SL/L	Alcan, RA207LS	H.C. Starck, UF15
SL/M	Baikalox, CR15	H.C. Starck, UF15
SL/N1	Alcan, RA207LS	H.C. Starck, UF32
SL/N2	Alcan, RA207LS	H.C. Starck, UF45
SL/P	Alcan, RA207LS	H.C. Starck, UF15
SL/Q1	Alcan, RA207LS	ENEA
SL/Q2	Alcan, RA207LS	ENEA
SL/R	Alcan, RA207LS	–
SL/S	Alcan, RA207LS	H.C. Starck, UF15
SL/V	Alcan, RA207LS	H.C. Starck, UF32
SL/W	Alcan, RA207LS	H.C. Starck, UF45

powders manufactured by H.C. Starck, and so no adjustments were made.

3. Results and discussion

3.1. Wet ball milling trials on alumina powders

Particle size data showed the immediate break down of agglomerates at the start of milling. The volume percent particle size data gave a value of 1.65 μm for the particle diameter at which 90% of the particles were smaller than (d_{90}), which reduced to 1.45 μm in the first 16 h. The d_{50} data showed a decrease from 0.50 to 0.45 μm over the same period. This reduction in particle size in turn lowered the comminution rate; whilst d_{90} continued to fall, d_{50} remained constant. These observations are in agreement with those made by other workers.[13] Owing to the probability dependency of the milling process, further significant reduction in particle size only occurred after an additional milling period. In the present study this was seen to be beyond 36 h, where d_{50} began to fall again, dropping to 0.4 μm after 46 h milling time.

Fig. 4 shows the variation in viscosity as a function of shear stress for different milling times for an RA207LS slurry. It can be seen that the slurry viscosity increases between 43 and 46 h milling, which may be due to one or a combination of two processes. Firstly, as the surface area of the powder increases, more polymer will be required to adsorb onto the surface of the particles to maintain a stable slurry. If insufficient polymer is available, particles may flocculate and cause the viscosity to increase. Secondly, it is possible that the abrasive action of the media causes degradation of the polymer, as described by Chartier et al.[14] Degradation is thought to occur through the dehydration of the polymer via the following reaction:

$$R - COO^{-}NH_4^{+} \rightarrow R - CO - NH_2 + H_2O \quad (1)$$

followed by its desorption from the alumina surface. Although the Versicol K11 used here is not in the ammonium salt form, as used by Chartier et al.,[14] ammonium ions will be present from the initial pH adjustment. The addition of excess polymer will serve as a suitable countermeasure and addresses the problem of insufficient coverage. Therefore, the correct amount of polymer, for a particular milling period, must be determined.

The optimum milling time was determined to be beyond 36 h, from the particle size analysis results. However, due to the possible effects of prolonged milling on the dispersant, it was decided to introduce a maximum milling time of 44 h. All 'batch' slurries used for pressure filtration were milled for 41 ± 1 h. Owing to the fineness of the CR15 powder, a proportion of the powder lay under the minimum detection size of 0.1 μm for the particle size analyser. Therefore, the same milling times as used for the RA207LS powder were adopted.

Comparison of the flow curves for an alumina slurry with 1 wt.% Dispex A40 and 1 wt.% Versicol K11 reveal a more pronounced shear thinning behaviour and slight thixotropy for the former; refer to Fig. 5. This behaviour is due to the lower molecular weight molecules in Dispex A40, which extend shorter distances from the particle surfaces. At pH values $\geqslant 8.5$ experimental evidence shows that poly methacrylic acid, with

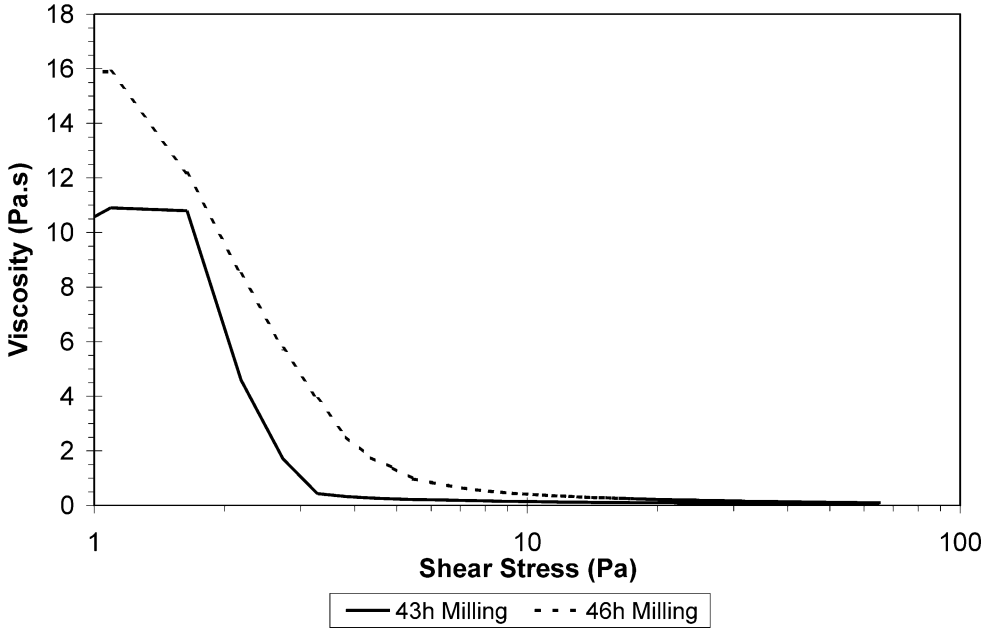

Fig. 4. The variation in viscosity as a function of shear stress for different milling times for an RA207LS slurry.

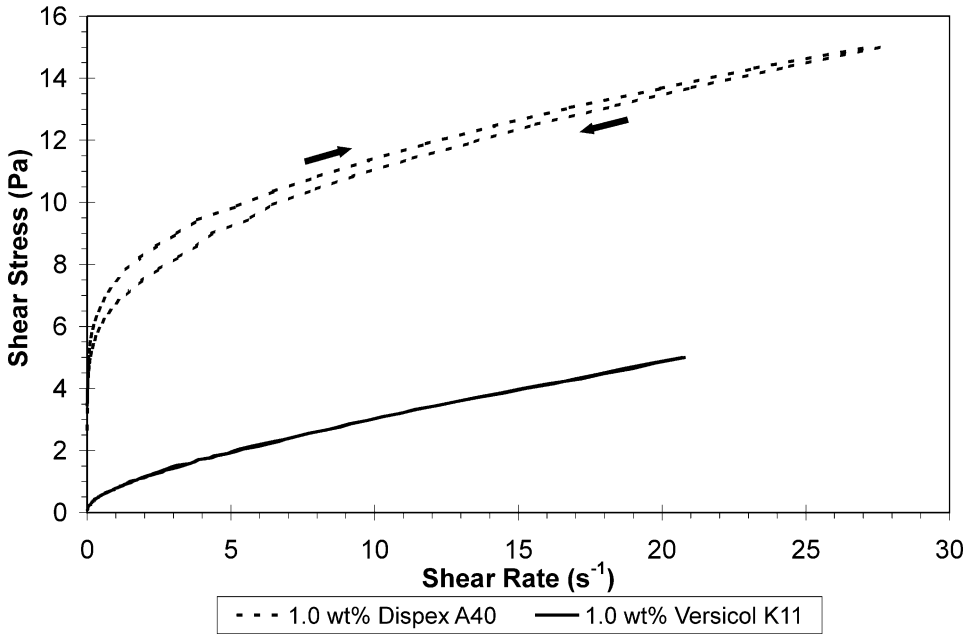

Fig. 5. Flow curves for RA207LS slurries containing Dispex A40 and Versicol K11.

Table 2
Magnitude of van der Waals interaction energy at the effective particle separation for Dispex A40 and Versicol K11

Dispersant	Effective particle separation (nm)	van der Waals interaction energy at effective particle separation (kT)[a]
Dispex A40	4.0	57.9
Versicol K11	13.3	14.3

[a] van der Waals values are for 0.5 μm diameter alumina particles in water.

an average molecular weight of 15,000, is in the form of expanded coils of approximately 10 nm in size (cited by Cesarano et al.[15]). This value was used in the present work to approximate the effective particle separation due to the presence of the adsorbed polymer layer for both dispersants; refer to Table 2. The value of the effective separation was calculated based on the assumption that the extension of the polymer will be in proportion to molecular weight, and that Dispex A40 and Versicol K11 are the same polymer[2] as that used by Cesarano et al.[15] The table reveals there to be a difference in the van der Waals force of attraction of over four times between Dispex A40 and Versicol K11. Depending on the magnitude of the electric double layer repulsive forces, this may well lead to the formation of flocs, due to secondary coagulation.

[2] Cesarano et al.[15] used the sodium salt of poly methacrylic acid. Dispex A40 differs in that there is not methyl group in the monomer unit, as is made from poly acrylic acid. Versicol K11, although 75 wt.% poly methacrylic acid, does not contain 25 wt.% poly acrylic acid.

At the low stress ranges used in the viscosity measurements, the shear stress required will be significantly dependent on the interparticle forces. The viscosity results in Fig. 5 show that Dispex A40 is unsuitable, since the initial shear stress required to mobilise the slurry (to give the same shear rate as the Versicol K11) is higher. It is also apparent, from the discussion so far, that the amount of dispersant used must be investigated. The time taken from stopping the mill to adding a sample to the vessel in the particle size analyser is a matter of minutes. It is therefore unlikely that appreciable re-agglomeration can occur since the stability of colloidal systems is time dependent. The sample vessel contains approximately 2 l of water and so when only a few drops of slurry is added from a disposable pipette the distance between particles becomes very large. Calculations were carried out as part of this work to quantify these distances; refer to the Appendix. The results show that the van der Waals interaction energy is greatly reduced when slurry is added to the sample vessel in the particle size analyser. Owing to these two factors, the relative merits of the slurries cannot be inferred. Measurements must be performed on the slurry in their natural state; that is, at their original volume loading. Therefore, viscosity results must be examined in order to make a better judgement on the state of dispersion. This formed the basis of the next series of experiments to optimise the amount of Versicol K11 dispersant used for the CR15 and RA207LS aluminas.

3.2. Optimisation of alumina slurry rheology

An addition of 4.5 wt.% dispersant gave the lowest viscosity at low shear stress (less than 5 Pa) for the

CR15 alumina. Similarly, for the case of the RA207LS system, 1.6 wt.% dispersant gave the optimum flow properties at low stresses (less than 2 Pa). The arbitrarily assigned low shear stress range is based on how flow behaviour is controlled by the interaction forces between particles. A minimum viscosity curve arises due to an optimum state of dispersion within the slurry, due to the competition between dispersion and flocculation forces/mechanisms. Hydrodynamic forces are more significant at higher shear rates[16] and so above the designated low stress range the viscosity of the slurry will increase proportionally with the viscosity of the dispersing medium.

3.3. Slurry batch production of nanocomposites

Fig. 6 shows typical flow curves for an RA207LS slurry, both before and after the UF15 silicon carbide was added. Both systems exhibit an initial shear thinning behaviour, with slight thixotropy. The low 'apparent' yield stress of the alumina curve indicates good dispersion of the alumina particles after milling.

The initial shear thinning characteristic is attributed to the disturbance of an ordered particle network. Calculations based on the modelling the positions of the particles as for simple lattices are presented in the Appendix. For a face-centred cubic arrangement of particles with a radius of 250 nm, for example, the minimum particle separation distance will be 70 nm at 50 vol.% solids loading (refer to Fig. A3). However, in order for particles to move past each other, particle rearrangement must occur. A consideration of the unit cell geometry (based on the calculations in the Appendix) reveals that particles can move past one another in 3 of the ⟨112⟩ directions, since a separation, x of only 22 nm is required. Particles cannot move past each other in the remaining 3 ⟨112⟩ directions because an *additional* 42 nm is required. The thixotropic nature of the curve is due the sol requiring time to recover its more ordered arrangement when the deforming stress is reduced.

The composite flow curve exhibits a higher yield stress with a larger thixotropic 'envelope'. Both characteristics can be attributed to the increased solids content of the slurry, resulting from the addition of the silicon carbide, which would reduce the separation distance between particles by a further 5 nm (based on the calculations in the Appendix). This treatment does assume that the silicon carbide has the same particle size as the alumina; this is a reasonable assumption for the RA207LS/UF15 system.

A comparison of the flow curves for the two ENEA silicon carbide systems and the SL/S system is given in Fig. 7, along with some data at low shear stress, to aid comparison. SL/Q1 has an extremely high yield stress, indicating a strongly agglomerated system. Although no appreciable flow was achieved at the shear stresses applied, shear destructive behaviour is likely at higher stresses. The mechanisms responsible for the agglomerates (addressed in the next section) are also responsible for the low thixotropy of this system, since they cause rapid reformation of agglomerates when the shear stress is reduced.

The SL/Q2 slurry is highly thixotropic, with a higher yield stress than the SL/S sol. This is indicative of a weakly flocculated system because the flocs are broken down at low shear stresses and have a lower 'driving

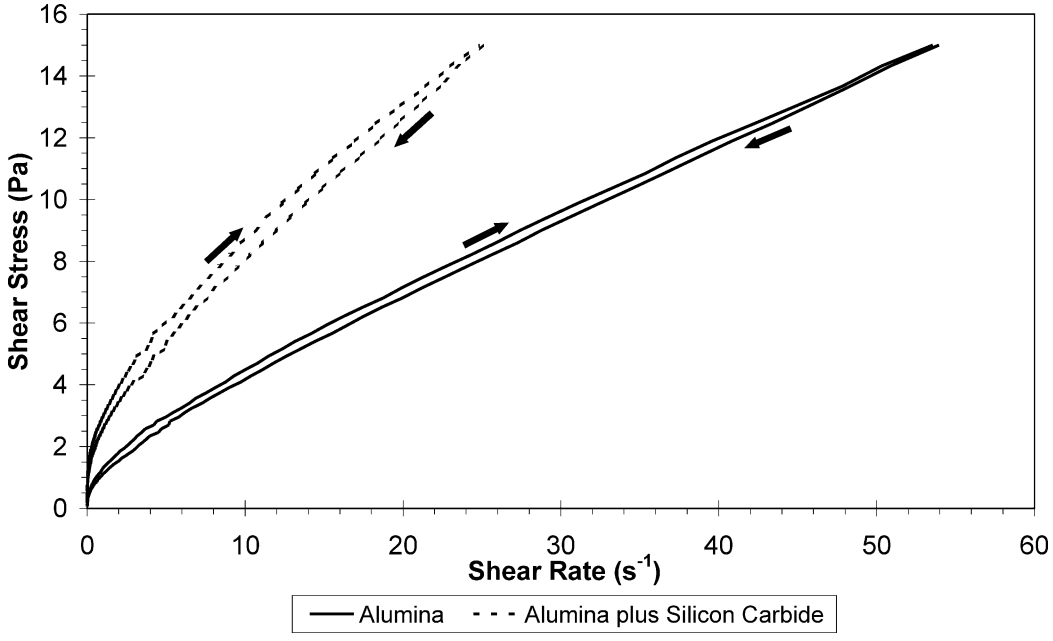

Fig. 6. Flow curves for SL/S before and after the addition on the UF15 silicon carbide.

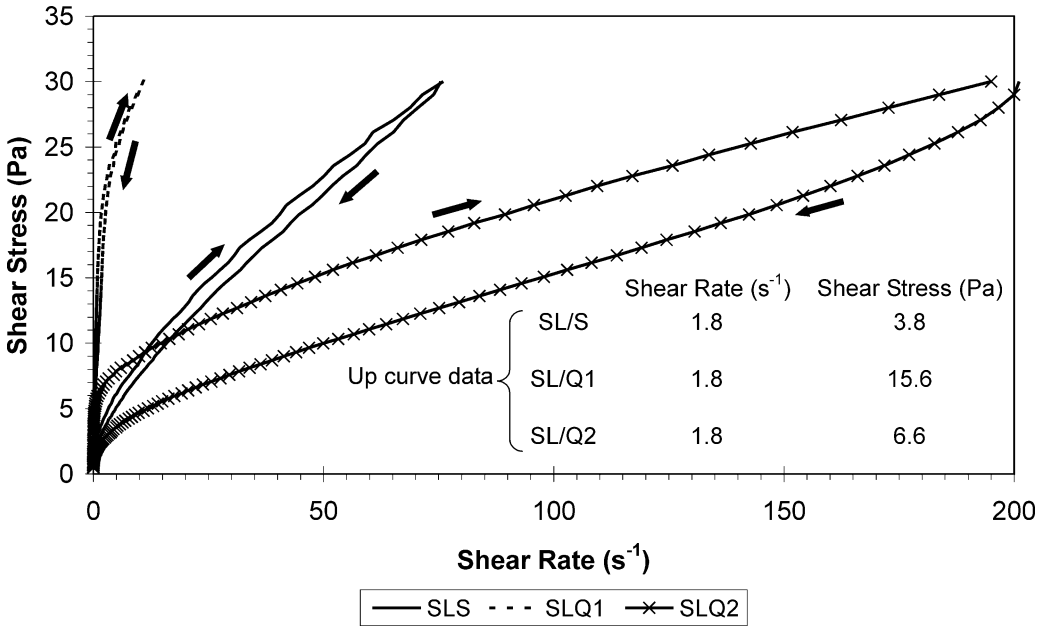

Fig. 7. Flow curves for composite slurries: SL/S, SL/Q2 and SL/Q1.

force' for reformation on the removal of the deforming stress. The viscosity in the linear part of the curve is lower than that of the SL/S slurry, which is most probably due to the lower solid content of the SL/Q2 slurry.

3.4. General discussion on 'sol architecture'

The arrangement of the alumina and silicon carbide particles in a sol is of crucial importance for the subsequent development of the desired nanocomposite microstructure. The silicon carbide particles must be well dispersed because no sintering will occur between them at the temperatures experienced in the subsequent heat treatments. Any silicon carbide agglomerates present may act as critical defects, or hinder densification causing other strength limiting flaws in the material. The term sol architecture shall be applied to denote the spatial arrangement of alumina and silicon carbide particles in the slurry.

For the case of RA207LS alumina and 5 vol.% UF15 silicon carbide, where the particle sizes are similar, there will be approximately 19 alumina particles for every silicon carbide particle; refer to Table 3. For the same alumina, but with 5 vol.% ENEA silicon carbide, the number of silicon carbide particles will outnumber the alumina particles at a ratio of 53 to 1. Therefore, producing a suitable sol architecture will be more difficult in the case of the ENEA powder systems. This is because, even if the powder is fully dispersed initially, there is a much higher probability of ENEA silicon carbide particles approaching each other and flocculation taking place.

Fig. 8 shows the results of an investigation into the sol architecture of an RA207LS/UF15 system. Since the size of the two powder types is similar, TEM wavelength

Table 3
Particle size data for the different silicon carbide types

Silicon carbide type	Particle size[a] (μm)	Number of RA207LS particles per silicon carbide particle[b]
H.C. Starck UF15	0.50	19
H.C. Starck UF32	0.35	7
H.C. Starck UF45	0.20	1
ENEA	0.05 (1/0.019 = 53)	0.019

[a] Data for the Lonza materials are the average of values obtained from the literature. ENEA particle size obtained from TEM micrographs.

[b] This assumes a monosized system, with an alumina particle size of 0.5 μm; figures based on the calculations presented in Appendix.

dispersive X-ray emission spectroscopy (WDX) was used to determine whether a particle was alumina or silicon carbide. Fig. 8(c) shows the spectrum obtained from a randomly chosen area, shown by the TEM micrograph in Fig. 8(a), which reveals peaks corresponding to the presence of both alumina and silicon carbide. Fig. 8(b) is a schematic diagram of the micrograph in (a), with the locations of the two spectra shown in (d) and (e) indicated. From the total number of approximately 20 grains examined, only one dominant Si peak was found [spectrum (d)]. This demonstrates that the theoretical situation for a dispersed system, discussed above, applied in this instance. The spectrum obtained in (e) shows the effect of the overlap of a touching alumina and silicon carbide grain.

TEM micrographs of the RA207LS/ENEA systems are shown in Figs. 9 and 10. The silicon carbide in the SL/Q1 slurry, milled at high pH (around pH = 9.2), is extensively agglomerated [Fig. 9(a)], with areas containing

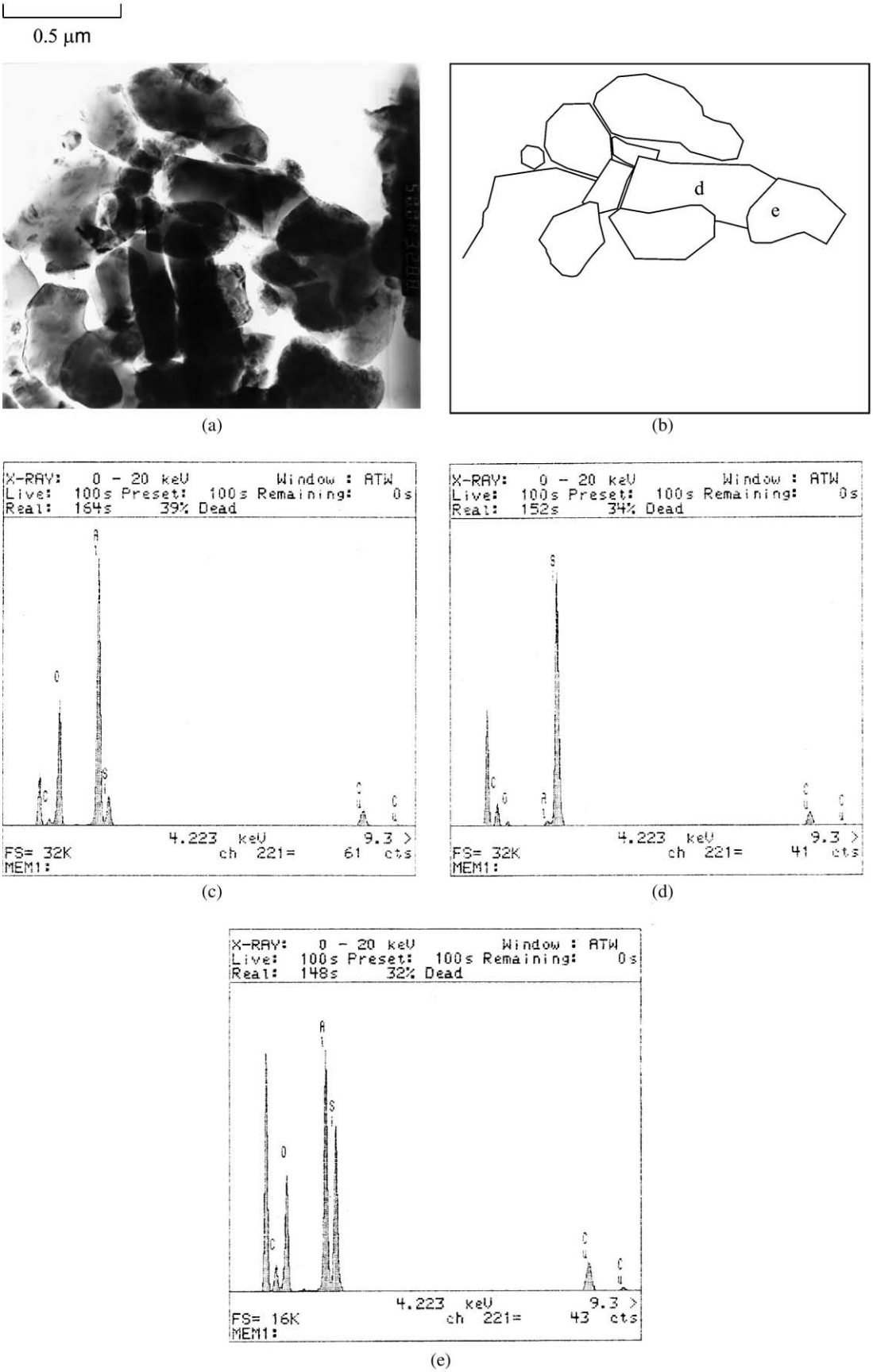

Fig. 8. TEM micrograph and associated WDX traces for an RA207LS/UF15 slurry.

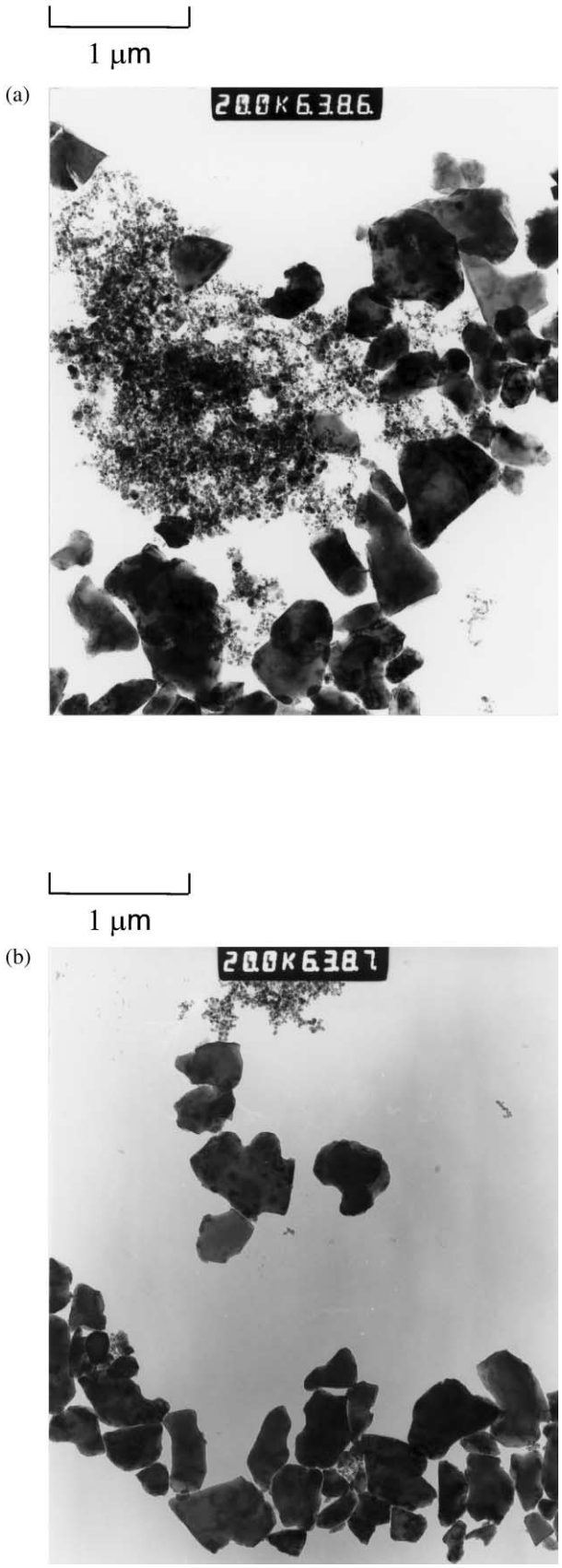

Fig. 9. TEM micrographs of SL/Q1 slurry showing (a) an area of extensive silicon carbide agglomeration and (b) an area predominantly free of silicon carbide.

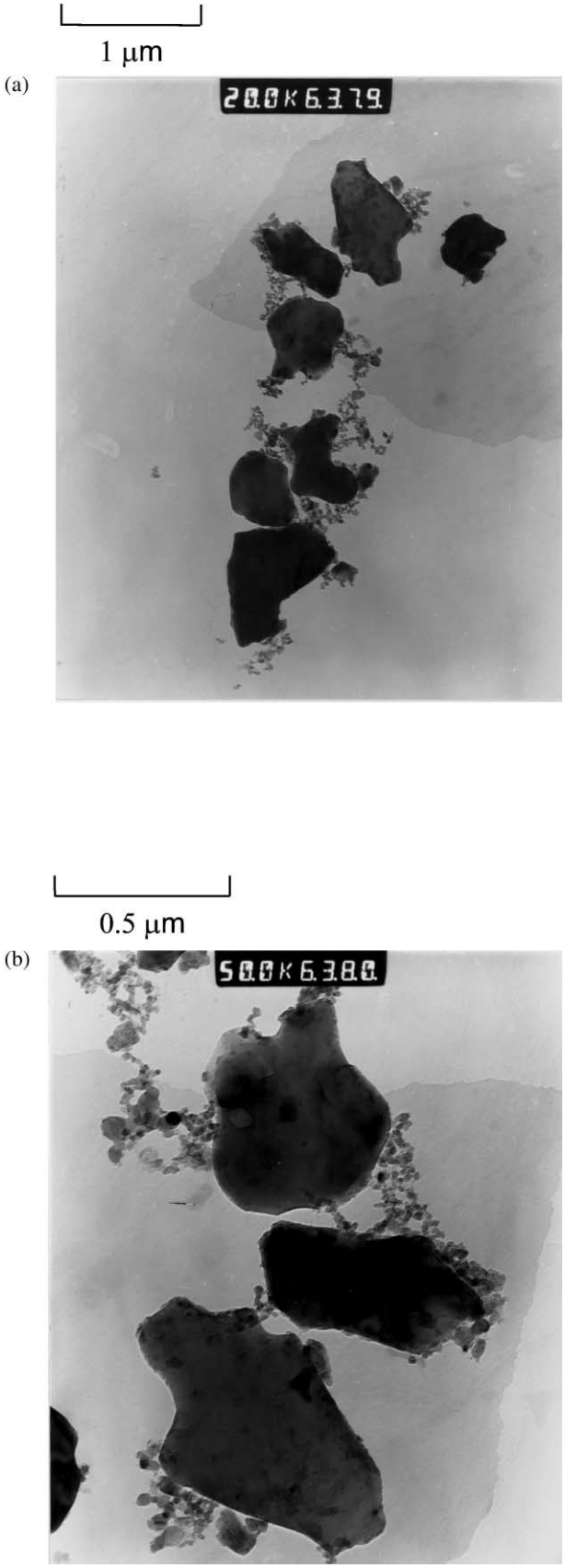

Fig. 10. TEM micrograph of SL/Q2 slurry showing (a) good dispersion of silicon carbide and (b) at higher magnification, where individual particles can be counted.

no silicon carbide [Fig. 9(b)]. The SL/Q2 slurry shows a much better dispersion of the silicon carbide, with an indication of heterocoagulation [Fig. 10(a)]. The number of silicon carbide particles can be counted more easily at higher magnification [Fig. 10(b)], revealing the correct proportion of silicon carbide particles to alumina as calculated above.

In order to understand the reasons behind the different sol architectures examined it is necessary to consider the chemical environment of the surface of the particles and the associated surface forces present. The alumina particles shall be considered first.

Fig. 11 shows the zeta potential for RA207LS plus a nominal amount of Versicol K11 dispersant as a function of pH. Measurements were performed using a Coulter Delsa 440 electrophoretic light scattering analyser; a detailed treatment of the equipment is given by Brownie.[17] The sol tested was diluted from a standard alumina slurry with 1 wt.% Versicol K11 to give a solid content of 2 vol.% and the pH adjusted with concentrated nitric acid and ammonia. The results obtained for a typical Bayer alumina, performed by Wei et al.,[18] also using electrophoresis are included for discussion purposes. At low pH (<3) the polymer will effectively be neutral and the zeta potential will be that due to the positive surface of alumina, but with reduced magnitude due the 'screening' effect of the adsorbed polymer layer. As the pH is increased, the functional groups along the length of the polymer will become dissociated and an increasing negative charge on the polymer will result (refer to Section 2.2 and Fig. 1). Cesarano and Aksay[12] have introduced the concept of an index (RNS) to measure the relative number of dissociated COO^- sites. The RNS was calculated by multiplying the amount of adsorbed PMAA by the fraction of COOH groups dissociated. The RNS was determined to be at its maximum at pH = 6.5. The zeta potential of alumina decreases at this point, which combined with the RNS of the added polymer, gives rise to the sharp change in the zeta potential of the alumina plus dispersant results in Fig. 11. At higher pH values, the magnitude of the zeta potential decreases as less polymer is adsorbed onto the alumina surface. The combined effect of the negative alumina surface at high pH and negatively charged dispersant give rise to a larger negative zeta potential than that with no dispersant added.

The IEP for the H C Starck type silicon carbide is pH = 3,[6] and the zeta potential will be negative for the conditions used to prepare slurries from this powder at pH ≅ 9.2. The adsorption of Versicol K11 onto silicon carbide has not been investigated, but any adsorption would serve to enhance the zeta potential, with the added provision of a steric barrier. The milling stage serves to disperse the silicon carbide, with the electrosteric barrier around the alumina particles preventing flocculation. As discussed earlier there are up to approximately 19 alumina particles associated with each UF15 silicon carbide particle in the RA207LS/UF15 system, limiting any silicon carbide/silicon carbide interactions. The result is the attainment of a well-dispersed sol, evidenced by Figs. 7 and 8.

A different situation to that outlined above arises for the case of the ENEA silicon carbide powder. Owing to the much smaller particle size of this powder, it has a very high surface area and so requires an increased volume of water to disperse individual particles. However, simply adding more liquid, it seems, is only part of the solution for achieving a good dispersion of the second phase.

At high pH, the polymer adsorbs onto the alumina in a relatively flat conformation, with each chain covering a relatively large surface area.[15] The silicon carbide will also carry a negative charge and so repulsion will result between the alumina/dispersant and silicon carbide. The

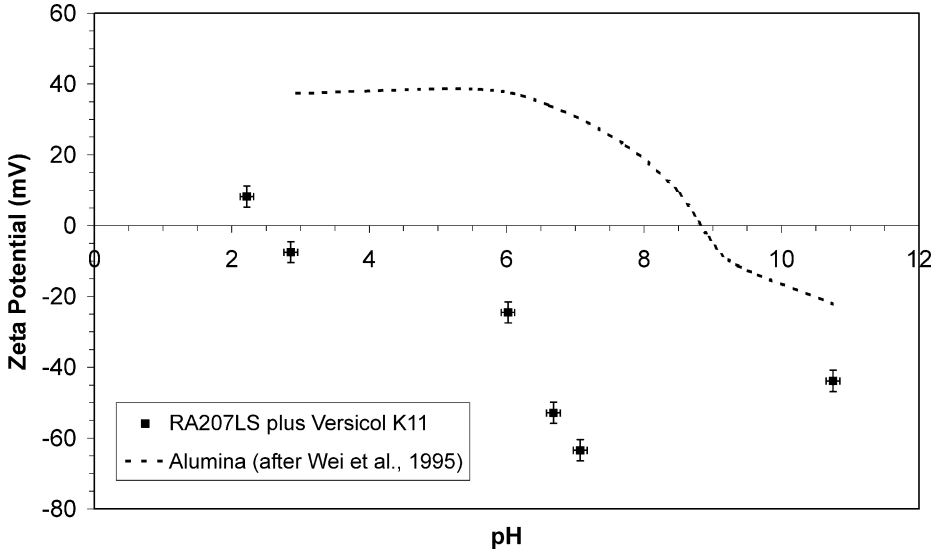

Fig. 11. Zeta potential of RA207LS powder with 1 wt.% Versicol K11 dispersant.

initial agglomerates from the dry powder are broken down to form smaller agglomerates, as shown by the TEM micrograph in Fig. 9(a). It is believed that further breakdown of the silicon carbide agglomerates is prevented by the repulsion between the agglomerates and the surrounding alumina particles, with the alumina particles effectively holding the cluster of silicon carbide particles together. The local viscosity of the liquid may also be high because at high pH there is more polymer in solution. This would limit ingress of liquid into the agglomerate and thus the action of any possible dispersion mechanisms. Furthermore, since the polymer chains are in an extended conformation, bridging flocculation effects around the outside surface of the clusters is likely. The result is a poorly dispersed system, as indicated by the flow curve in Fig. 7. The SL/Q1 slurry was 'streaky' in appearance, with white and black bands evident. These bands correspond to the two different powder types and illustrate the severity of the agglomeration in the silicon carbide powder. All other slurries were uniform in colour, as viewed by the naked eye.

At low pH (pH $\cong$ 5.8) the degree of dissociation falls and there is less repulsion between different sections of the polymer length, giving rise to a looped conformation. Reduced dissociation also means that there is a lowering of the electrostatic barrier, manifested as a lowering of the zeta potential as seen in Fig. 11. In addition, the amount of adsorbed polymer increases with decreasing pH to such an extent that the excess polymer in solution at high pH may be totally adsorbed onto the alumina surface.[15] The overall surface charge of the alumina will be positive, but the silicon carbide will be negative since it has a lower IEP. A model is now proposed for the sol architecture of the SL/Q2 system, based on this information.

The model is based on the fact that the reduction in pH gives rise to increased adsorption of the polymer. Since the amount of dispersant was tailored to suit the alumina milling stage at high pH and no subsequent additions of Versicol K11 were made, insufficient coverage of the particle surface will result at low pH. Consequently, patches of the alumina surface are created with no polymer barrier. The fine, negatively charged silicon carbide particles are thus attracted to the positive, polymer free patches, on the alumina surface; giving rise to heterocoagulation; refer to Fig. 12. A combination of this mechanism and the milling action will serve to break up the ENEA powder clusters, present from the powder in its dry form. Just as the zirconia media will disperse the alumina particles, the alumina particles will serve to disrupt the silicon carbide agglomerates. The result is shown clearly in Fig. 10, revealing good dispersion of the silicon carbide particles. The thixotropic nature of the SL/Q2 slurry, shown in Fig. 7, is thought to derive from the weak flocs formed between the alumina particles because of the reduced electrosteric barrier.

Figs. 13 and 14 show the striking differences between the colour homogeneity of green samples produced from the two ENEA systems. The picture on the left of each figure is the surface originally in contact with the filter assembly, with the opposite face shown on the right hand side. The extensive silicon carbide agglomeration in the

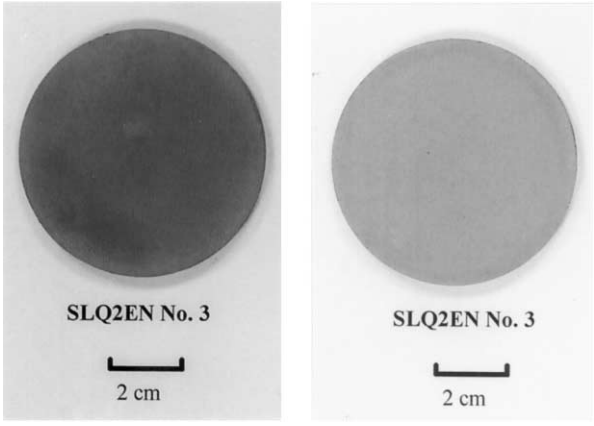

Fig. 13. Photograph of a green compact formed from the SL/Q1 slurry.

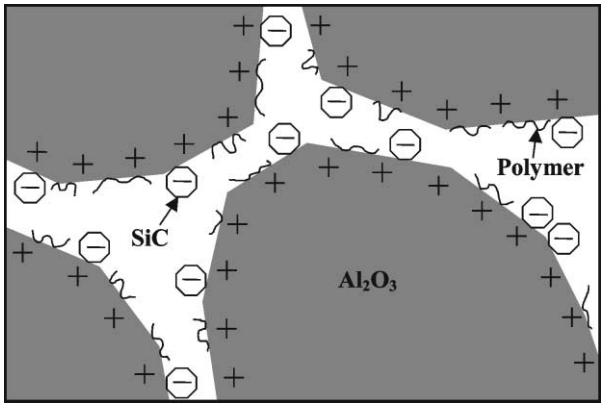

Fig. 12. Schematic of the proposed 'sol architecture' in the RA207LS/ENEA system processed at low pH.

Fig. 14. Photograph of a green compact formed from the SL/Q2 slurry.

SL/Q1 system manifests itself as a streaked appearance due to the alumina and silicon carbide rich areas. The SL/Q2 discs are typical of all the other composite specimens (regardless of source), exhibiting an even colouration that is indicative of good second phase dispersion.

4. Conclusions

The studies on colloidal processing, for the preparation of alumina/silicon carbide nanocomposites, have demonstrated that dispersed sols can be prepared with silicon carbide powders having an average particle size ranging from 0.5 μm down to 50 nm. Whilst a polydispersion approach is suitable for the coarser H.C. Starck powders, it cannot be applied to the very fine ENEA powder. However, a heterocoagulation route provides a solution for the processing of very fine silicon carbide, and provides an alternative to more complex methods using polymeric precursors. An explanation has been offered for the underlying mechanisms in terms of discussing the sol architecture.

Acknowledgements

The authors thank the Engineering and Physical Sciences Research Council and BG Technology for funding this research via a PhD CASE award for L.A.T., and Professors M.H. Loretto and I.R. Harris of the IRC in Materials and the School of Metallurgy and Materials, respectively, for the provision of laboratory facilities. Our gratitude also goes to ENEA, Italy (via Dr. E. Borsella) for the supply of the silicon carbide powder.

Appendix. The effect of the volume loading of the solid phase in a sol on the minimum separation distance

If the particles in the sol are assumed to be monosized, spherical and arranged regularly in a cubic cell, an informative approximation of the minimum average separation between particles can be obtained. The three geometries considered; simple cubic (SC), body centred cubic (BCC) or face centred cubic (FCC), are shown schematically in Fig. A1.

All cells have an edge length a, and thus volume a^3. In order to calculate the *minimum* average separation, a close packed plane in each cell must be chosen, as indicated by the shaded areas in Fig. A1. The two-dimensional sections along these planes and associated dimensions are shown in Fig. A2, where x is the minimum average separation and r is the particle radius.

For the simple cubic system:

$$a = 2r + x \tag{A1}$$

For the body centred cubic system:

$$a = \frac{4r + 2x}{\sqrt{3}} \tag{A2}$$

For the face centred cubic system:

$$a = \frac{4r + 2x}{\sqrt{2}} \tag{A3}$$

The solids volume loading of the cell and thus the sol, L, assuming all space between particles is filled with liquid, will be given by the following general relationship:

$$L = \frac{n4\pi r^3}{3a^3} \tag{A4}$$

where n is the number of whole particles per unit volume, a^3. From Fig. A1 it can be seen that $n = 1$ for a SC system, $n = 2$ for a BCC system and $n = 4$ for a FCC system.

Substituting Eq. (A1) into Eq. (A4) gives:

$$L = \frac{4\pi r^3}{3(2r + x)^3} \tag{A5}$$

for a simple cubic arrangement of particles.

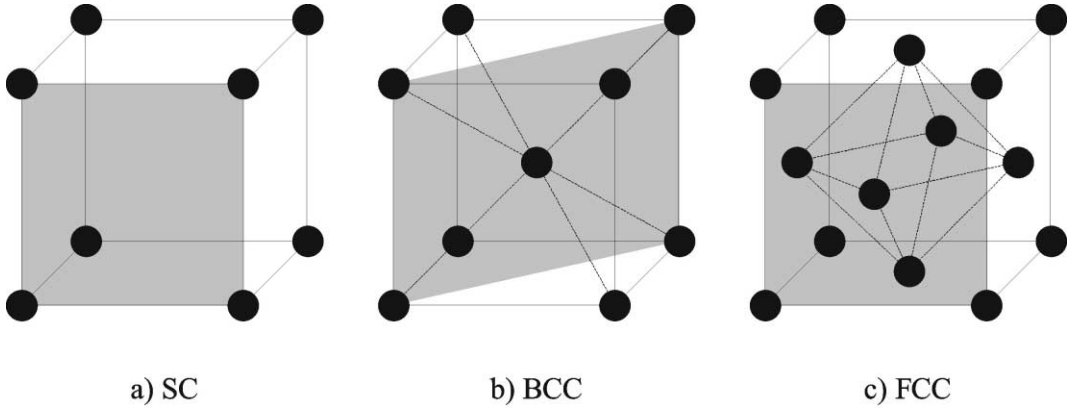

Fig. A1. Three cubic cell arrangements that can be used to model the average minimum separation between sol particles.

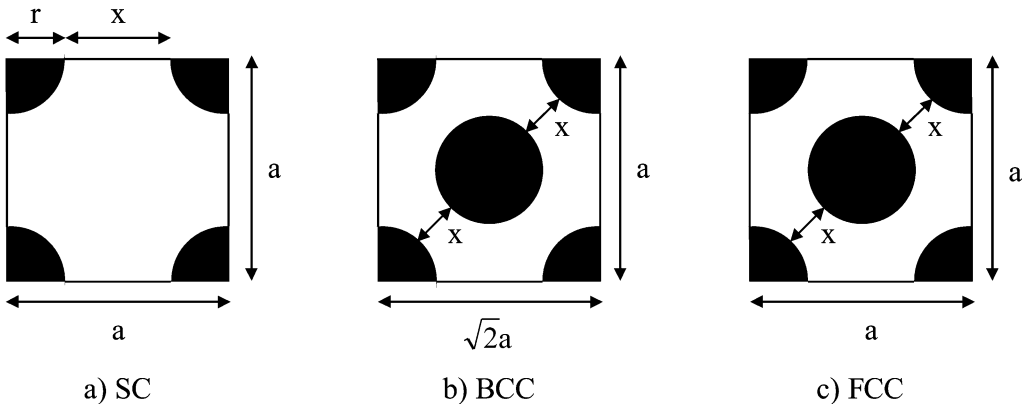

Fig. A2. Two-dimensional cross-sections of the a close packed planes from Fig. A1.

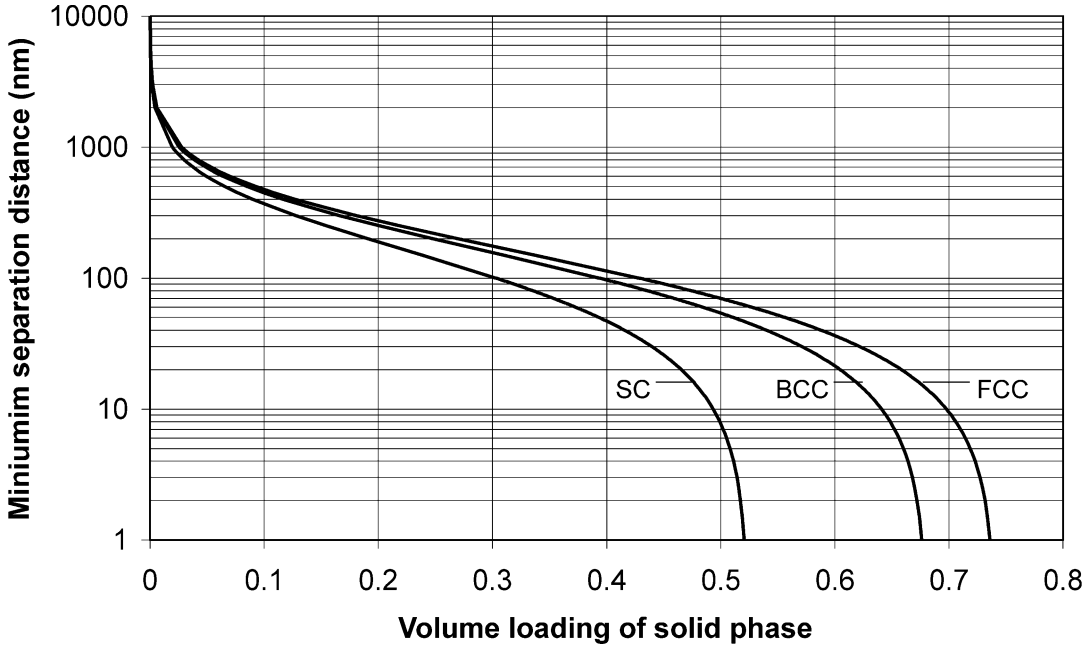

Fig. A3. Variation in minimum separation distance with solids loading for different sol 'cell geometry's' for 0.5 μm diameter particles.

Table A1
Separation distance and van der Waals interaction energy at different solids content

Packing type	0.005 Vol.% solids loading		50.0 Vol.% solids loading	
	Average minimum separation (nm)	van der Waals interaction energy (kT)	Average minimum separation (nm)	van der Waals interaction energy (kT)
SC	10438.9	3.2×10^{-9}	7.8	27.4
BCC	11436.6	1.9×10^{-9}	54.0	1.9
FCC	16656.96	2.2×10^{-10}	69.9	1.2

Substituting Eq. (A2) into Eq. (A4) gives:

$$L = \frac{8\pi r^3}{3\left(\frac{4r+2x}{\sqrt{3}}\right)^3} \quad \text{(A6)}$$

for a body centred cubic arrangement of particles.

Substituting Eq. (A3) into Eq. (A4) gives:

$$L = \frac{16\pi r^3}{3\left(\frac{4r+2x}{\sqrt{2}}\right)^3} \quad \text{(A7)}$$

for a face centred cubic arrangement of particles.

Fig. A3 shows the results of Eqs. (A5), (A6) and (A7) graphically, for a particle radius of 0.25 μm.

Table A1 shows the separation distance and van der Waals force of interaction at solids contents of 0.005 and 50 vol.%. The former solids loading corresponds to that found typically in the Coulter LS130 particle size analyser and the latter to that of a typical slurry. It is obvious that the van der Waals force of interaction is negligible at 0.005 vol.% solids content, compared with that at 50 vol.%, due to the large separation distances that exist between particles.

References

1. Niihara, K., New design concept of structural ceramics: ceramic nanocomposites. *J. Ceram. Soc. Jpn, Int. Ed.*, 1991, **99**, 945–952.
2. Niihara, K. and Nakahira, A., Strengthening and toughening mechanisms in nanocomposite ceramics. *Ann. Chim. Fr.*, 1991, **16**, 479–486.
3. Niihara, K. and Nakahira, A., Particulate strengthened oxide ceramics-nanocomposites. In *Advanced Structural Inorganic Composites*, ed. P. Vincenzini. Elsevier Science Publishers, 1991, pp. 637–644.
4. Stearns, L. C., Zhao, J. and Harmer, M. P., Processing and microstructure development in Al_2O_3–SiC 'Nanocomposites'. *J. Eur. Ceram. Soc.*, 1992, **10**, 473–477.
5. Conder, R. J., Microstructure, *Processing and Properties of Nanocomposite Ceramics*. PhD thesis, University of Birmingham, 1994.
6. O'Sullivan, D., Poorteman, M., Descamps, P., Cambier, F., Leriche, A. and Thierry, B., Optimisation of alumina—silicon carbide dispersions and the fabrication of nanocomposite ceramic materials. In *Key Engineering Materials,* 99-100, ed. Trans. Tech. Publications, Switzerland, 1995, pp. 247–256.
7. Walker, C. N., Borsa, C. E., Todd, R. I., Davidge, R. W. and Brook, R. J., Fabrication, characterisation and properties of alumina matrix nanocomposites. In *British Ceramic Proceedings, No. 53: Novel Synthesis and Processing of Ceramics*, ed. F. R. Sale. The Institute of Materials, London, 1994, pp. 249–264.
8. Aslan, M., Dörr, Naß, R. and Schmidt, H., Microstructural development and mechanical properties of pressureless sintered Al_2O_3/SiC composites. In *Proceedings of the International Conference Ceramic Processing Science and Technology*. Friedrichshafen (Bodensee), FRG, 11–14 September, 1994, pp. 665–669.
9. Assmann, S., Eisele, U. and Böder, H., Processing of Al_2O_3/SiC composites in aqueous media. *J. Eur. Ceram. Soc.*, 1997, **17**, 309–317.
10. Baklouti, S., Pagnoux, C., Chartier, T. and Baumard, J. F., Processing of aqueous α-Al_2O_3, α-SiO_2 and α-SiC suspensions with polyelectrolytes. *J. Eur. Ceram. Soc.*, 1997, **17**, 1387–1392.
11. Fantoni, R., Borsella, E., Piccirillo, S., Ceccato, R. and Enzo, S., Laser synthesis and crystallographic characterisation of ultra-fine SiC powders. *J. Mater. Res.*, 1990, **5**(1), 143–150.
12. Cesarano, J. III and Aksay, I. A., Processing of highly concentrated aqueous α-alumina suspensions stabilized with polyelectrolytes. *J. Am. Ceram. Soc.*, 1988, **71**(12), 1062–1067.
13. Kerr, M. C. and Reed, J. S., Comparative grinding kinetics and grinding energy during ball milling and attrition milling. *Am. Ceram. Soc. Bull.*, 1992, **71**(12), 1809–1816.
14. Chartier, T., Souchard, S., Baumard, J. F. and Vesteghem, H., Degradation of dispersant during milling. *J. Eur. Ceram. Soc.*, 1996, **16**, 1283–1291.
15. Cesarano III, J., Aksay, I. A. and Bleier, A., Stability of aqueous α-Al_2O_3 suspensions with poly(methacrylic acid) polyelectrolyte. *J. Am. Ceram. Soc.*, 1988, **71**(4), 250–255.
16. Barnes, H. A., Hutton, J. F. and Walters, K., *An Introduction to Rheology*. Elsevier Science Publishers BV, 1989.
17. Brownie, P. M., PhD thesis, The University of Birmingham, 1995.
18. Wei, W. J., Lu, S. J. and Yu, B., Characterisation of submicron alumina dispersions with poly(methacrylic acid) polyelectrolyte. *J. Eur. Ceram. Soc.*, 1995, **15**, 155–164.